RSC Advances

ROYAL SOCIETY OF CHEMISTRY

www.rsc.org/advances

Journal Name

ARTICLE

In-situ fabrication of highly crystalline CdS decorated Bi_2S_3 nanowires (Nano-Heterostructure) for visible light photocatalyst application

Received 00th January 20xx,
Accepted 00th January 20xx

DOI: 10.1039/x0xx00000x

www.rsc.org/

Rajendra P. Panmand[a]*, Yogesh A. Sethi[a], Rajashree S. Deokar[b], Datta J. Late[c], Haribhau M. Gholap[b], Jin Ook Baeg[d] and Bharat B. Kale[a]**

In-situ synthesis of the orthorhombic Bi_2S_3 nanowires decorated with hexagonal CdS nanoparticles (nano-heterostructure) has been demonstrated by facile solvothermal method. The tiny 5-7 nm CdS spherical nanoparticles are decorated on the surfaces of 30-40 nm Bi_2S_3 nanowires, successfully. Structural, morphological and optical study clearly shows the existence of CdS on Nanowires. A possible sequential deposition growth mechanism is proposed on the basis of experimental results to reveal the formation of the nano heterostructure. The heterostructures have been used as photocatalyst for hydrogen production as well as degradation of Methylene Blue under solar light. The maximum hydrogen evolution i.e. 4560 and 2340 µmol/hr/0.5g was obtained from H_2S splitting and glycerol degradation for Bi_2S_3 NWs decorated with CdS nanoparticles (nano-heterostructure) which is higher than that of the Bi_2S_3 NWs (3000 and 1170 µmol/hr/0.5g, respectively). The enhanced photocatalytical hydrogen evolution efficiency of heterostructures is mainly attributed to its nanostructure. In the nano heterostructure, the CdS nanoparticles control the charge carrier transition, recombination, and separation, while the Bi_2S_3 nanowire serves as support for the CdS nanoparticles. The photogenerated electron's migration is faster than the holes from the inside of a CdS nanoparticles to its surface or to the phase interface, resulting in relatively higher hole density inside the CdS nanoparticle leaving electron density at surface of Bi_2S_3 NWs. This influences the photocatalytic activity under solar light. Such nano-heterostructures may have potential in other photocatalytic reactions.

1. INTRODUCTION

One-dimensional (1D) oxide and sulphides nanostructures, such as nanorods, nanotubes, nanowires and nanobelts, have attracted intensive interest due to their unique optical, electronic and mechanical properties, and potential application in the fabrication of photocatalyst, nanoscale electronics and optoelectronics devices.[1-3] One Dimensional (1D) semiconductors are considered as the most encouraging photosensitive materials due to the large surface-to-volume ratio and a Debye length comparable to their small size.[4,5] The number of surface trap states and prolong photo-carrier lifetime with increase of surface-to-volume ratio, ultimately enhance the photocatalytic performance of material.[6, 7]

The photocatalytic hydrogen generation as a clean energy via abundant water, hydrogen sulphide splitting and biomass degradation using semiconductor photocatalyst has attracted much attention due to the global energy crisis and environmental problems. Till date, most of the semiconductor photocatalysts have low efficiency and instability for hydrogen evolution under the solar light. In view of this, different semiconductor heterostructures[8-11] have been investigated and designed to enhance the photo-induced charge carrier's separation unlike to single phase photocatalysts.[12, 13]

Considering the importance of the one dimensional as well as heterostructured materials for photocatalysis, many efficient and stable heterostructures for photocatalytic hydrogen generation are investigated based on different electron transfer mechanisms.[14-18] For example, CdS/CeO_x heterostructures show superior hydrogen generation than single CdS or CeO_x due to the efficient light harvesting and fast separation of photogenerated carriers compared to CdS or CeO_x. Jum Suk Jang[19] and group have also reported that the molar concentration of TiO_2 in CdS NW/TiO_2 nanocomposite

[a] Centre for Materials for Electronics Technology (C-MET), Panchawati, Off Pashanroad, Pune-411008,India.
[b] Department Of Physics, Fergusson College, Pune – 411004, India.
[c] Physical and Materials Chemistry Division, CSIR-National Chemical Laboratory, Pashan Road, Pune 411008, India.
[d] Korea Research Institute of Chemical Technology, Division of Green Chemistry and Engineering Research, 100 Jangdong, Yusong, Daejon, KR 305-600, South Korea.
† Footnotes relating to the title and/or authors should appear here.
Electronic Supplementary Information (ESI) available: [details of any supplementary information available should be included here]. See DOI: 10.1039/x0xx00000x

photocatalyst exhibit highest activity for H_2 evolution. This configuration of photocatalyst results in an efficient charge separation due to fast diffusion of photoelectrons generated from CdS NWs toward surrounding TiO_2 NP, leading to high photocatalytic activity of hydrogen production. The CdS accompanied with host material such as ZnO and $CdLnS_4$, alter the energy levels of the conduction and valence bands in the coupled semiconductor system which helps to enhanced hydrogen generation via water splitting. [20, 21] Recently, Zhen Fang et al. demonstrated that a growth of CdS on Bi_2S_3 nanostructures may exhibit high hydrogen evolution by prolonging lifetime of charge carriers.[22] The heterostructured CdS/Bi_2S_3 has been also investigated for photocatalytic organic dye degradation and enhanced photoelectrochemical activity.[23-25] However, there are some issues regarding the synthesis and characterization of such heterostructure and is very essential to skirmish them by thorough investigation. Also, photocatalytic hydrogen production using CdS/Bi_2S_3 has not been reported yet. In view of this, we have demonstrated CdS/Bi_2S_3 nano-heterostructure with formation and growth mechanism as well as with justified enhanced hydrogen evolution.

Recent studies on Metal Sulfides reveals that the group of highly efficient catalysts for photochemical reactions due to photogenerated charge carriers can rapidly move to the surface of the catalysts, reducing or oxidizing organic molecules. CdS nanostructures were demonstrated as an effective photocatalyst to degrade Methylene blue, methyl orange, and Rhodamine B under visible irradiation conditions.[26,27] Bi_2S_3nanostructures with different sizes show good activity in photodegradation of rhomdamine B.[28] Whereas the heterostructures like CdS/Bi_2S_3 also tested for degradation of Methylene Red.[22]

In the present work, we report synthesis of Bi_2S_3 nanowires (NW) decorated with CdS nanoparticles (nano-heterostructure) as an efficient photocatalyst for Methylene blue degradation and hydrogen evolution from hydrogen sulphide splitting and the Glycerol degradation. The Heterostructure has characterized thoroughly for their structural optical properties. The Bi_2S_3 nanowires decorated with CdS nanoparticles showed very stable hydrogen under the solar light which is hitherto unattempted.

2. Experimental

2.1 Materials and synthesis

All raw materials in our experiments were purchased from s. d. fine chemical ltd and used without further purification.

2.2 Synthesis of Bi_2S_3 NWs and Bi_2S_3 NWs decorated with CdS nanoparticles

In a typical procedure, 0.04 mole of anhydrous $BiCl_3$ added to 70 mL of Ethylene Glycol (EG) and the mixture was vigorously stirred to form a homogeneous solution. Simultaneously, 0.06 moles of Thioacetamide and 0.2 gm of Polyvinylpyrrolidone (PVP) were dissolved in the 10 ml of methanol. Both solutions were transferred into a 100 mL Teflon-lined autoclave. The autoclave was sealed, maintained at 120°C for 12 h, and cooled to room temperature naturally. The black precipitate was collected and washed three times with water and absolute ethanol, respectively. Then the sample was dried in a vacuum at 50°Cfor 2h.The same procedure has been followed to synthesize Bi_2S_3nanowires decorated with CdS with addition of 0.01 and 0.02mole of $Cd(NO_3)_2{\cdot}4H_2O$.

2.3 Characterization

The phase purity of the Heterostructure was investigated by XRD (Bruker (D8). Morphological study was performed using FESEM (Hitachi S-4800). Transmission Electron Microscopy (TEM) images and the corresponding selected area electron diffraction (SAED) patterns were obtained on a JEOL JEM-2010 instrument. Raman spectrum of the samples was performed using HR 800-Raman Spectroscopy, Horiba JobinYvon, France. The room-temperature UV-Vis absorption spectrum was recorded on a Perkin Elmer λ-950 spectrophotometer in the wavelength range of 200-800 nm.

2.4 Photo-response study

A photoresponse device was made by sandwiching an as prepared Bi_2S_3 NWs and Bi_2S_3 decorated with CdS nanoparticles in FTO glass substrate with a device configuration of FTO/Bi_2S_3-CdS/FTO as shown in the Figure ESI I. A Xenon Arc lamp (300W/cm^2) was used as the illumination source, and a bias voltage of 500 mV was applied on the FTO electrode. The light was interrupted at 15 s intervals, and the currents were measured at crono galvanostatic mode (Autolab, PGST30). With the light regularly chopped, current spikes were recorded.

2.5 Photocatalytic study for H_2S splitting

The cylindrical quartz photochemical thermostatic reactor was filled with 700 mL of 0.5 M aqueous KOH and purged with Ar for 1 h. H_2S was bubbled through the solution at a rate of 2.5 $mLmin^{-1}$ at 298 K. H_2S was continuously fed into the system during the photo-reduction. The 0.5 g sample was introduced into the reactor and irradiated with 300W visible light source with constant stirring. The UV light has been blocked using 420 nm optical filter. The excess H_2S was trapped in the NaOH solution. The amount of hydrogen evolved was measured using a graduated gas burette.

2.6 Photocatalytic study for Methylene Blue (MB) degradation

Photocatalytic activities of the samples were evaluated by the degradation of methylene blue (MB) under visible light irradiation using a same light source as mentioned above. In each experiment, 0.1 g of the photocatalyst was added to 600mL of MB solution (1 x 10^{-5} and 1.6x10^{-5} M, respectively). Before illumination, the suspensions were vigorously stirred in the dark for 1 h to ensure the establishment of an adsorption–desorption equilibrium between photocatalyst and dye. Then the solution was exposed to visible light irradiation. At certain intervals, a 10 mL solution was sampled and centrifuged to remove the remnant of photocatalyst. Finally, the adsorption

UV-vis spectrum of the filtrates was recorded using a λ-950 (Perkin Elmer) spectrophotometer.

2.7 Photocatalytic study for Glycerol degradation

The apparatus used for photocatalytic experiments consists of solar light-simulating source, quartz photoreactor and an on-line analysis system. Same light source is used for photocatalytic glycerol degradation, as mentioned above. The photoreactor is of cylindrical shape and its top cover has provisions for measurements of solution pH and temperature, as well as connections for inlet/outlet of the carrier gas (Argon). The gas outlet is equipped with a water-cooled condenser which does not allow vapors to escape from the reactor. The outlet of the reactor is connected to the measuring cylinder via CO_2 trap and further Hydrogen gas is collected and analysed on Gas Chromatography. The 1 gm of photocatalyst has been used for glycerol degradation.

3 Resultand Discussions

The phase purity and crystal structure of as-obtained Bi_2S_3 NWs and Bi_2S_3 NWs decorated with CdS was examined with powder XRD and shown in Figure 1A. The XRD pattern of Bi_2S_3NW is shown in Figure 1A (p) which shows existence of well-indexed orthorhombic Bi_2S_3 (JCPDS card No.17-0320: Figure 1B). After, addition of the 0.01 and 0.02 mole of $Cd(NO_3)_2$ in reaction, a new widened peak, denoted by an asterisk, appears at 2θ of 26.47° (Figure 1A (q), (r) and inset of Figure 1A),which originates from the characteristic reflection of (002) planes of hexagonal phase of CdS (JCPDS cardNo.41-1049: Figure 1C).From XRD pattern, it is also concluded that the intensity of (002) peak of CdS increased with increase in the concentration of $Cd(NO_3)_2$ (Figure 1A (r)). The relatively weak diffraction peak of CdS can be ascribed to the lower loading of CdS in the heterostructures.

The morphological studies of the nanostructures were investigated using Field Emission Scanning Electron Microscopy (FE-SEM). Figure2 shows FE-SEM images of the pristine Bi_2S_3 NW and Bi_2S_3NWs decorated with CdS. Figure 2 A and B shows typical FESEM image of the Bi_2S_3NWs, and most of them are 30-40 nm and few micrometres in length. Typical images of Bi_2S_3 NWs decorated with CdS are shown in Figure 2C-F. The Bi_2S_3NWs are decorated with 5-7nm CdS anoparticles (Figure 2 C & D) using 0.01 mole of the $Cd(NO_3)_2$.Figure 2 C and clearly shows rough surface of Bi_2S_3NW due to the growth of the CdS which is also confirmed by XRD.In images of samples obtained at higher concentration of $Cd(NO_3)_2$(0.02 mole), along with the 5-7 nm CdS, the bigger sized i.e. 60-70 nm CdS nanoparticles on Bi_2S_3NW sare also observed via secondary growth (Figure 2 E and F).At higher concentration, the crystal growth is quite faster due to higher ionic concentration. Hence, the bigger particle formation via secondary growth is quite obvious.

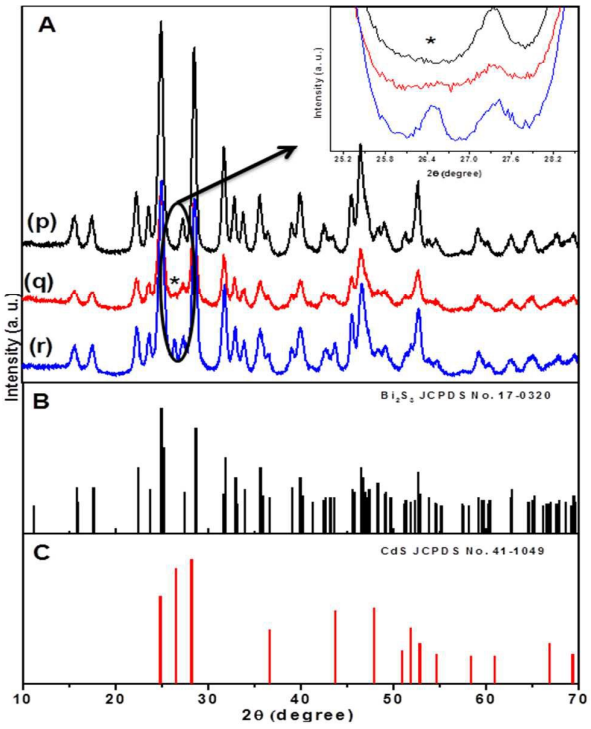

Figure 1:XRD patterns (A) of the as-obtained Bi_2S_3NW (p) and Bi_2S_3 NWS decorated with CdS ((q) and (r)).The JCPDS standard patterns of Bi_2S_3(B) and CdS(C).

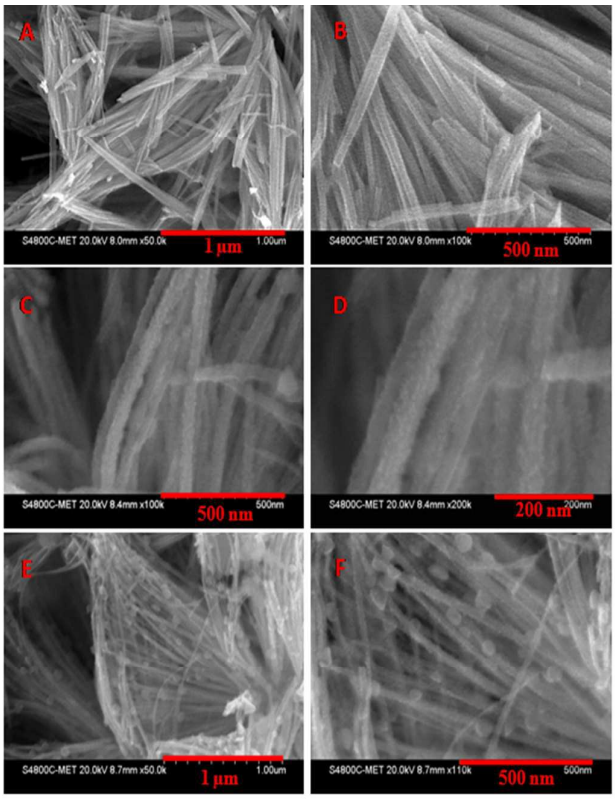

Figure 2: FESEM images of Bi_2S_3 NW (A and B), Bi_2S_3 NW decorated with CdS using 0.01 mole of $Cd(NO_3)_2 \cdot 4H_2O$ (C and D) and Bi_2S_3 NW decorated with CdS using 0.02 mole of $Cd(NO_3)_2 \cdot 4H_2O$ (E and F)

The microstructural information of the heterostructure was further analysed by HRTEM. HRTEM image (Figure 3) showsBi_2S_3 NW decorated with CdS using 0.01 mole of $Cd(NO_3)_2$.Figure 3 clearly reveals that the CdS nanostructures of size 5-7 nm are grown on the 30-40 nm Bi_2S_3 NW which is in agreement with FESEM results. Figure 3c and d clearly resolve the lattice fringes of the heterostructure. The interplanar spacing i.e. 0.33 nm can be indexed to the (002) planeof hexagonal CdS, while the 0.30nm correspond with that of the (211) lattice plane of orthorhombic Bi_2S_3. Thecorresponding SAED pattern of the heterostructure represents the single crystalline nature of material (Figure 3b).

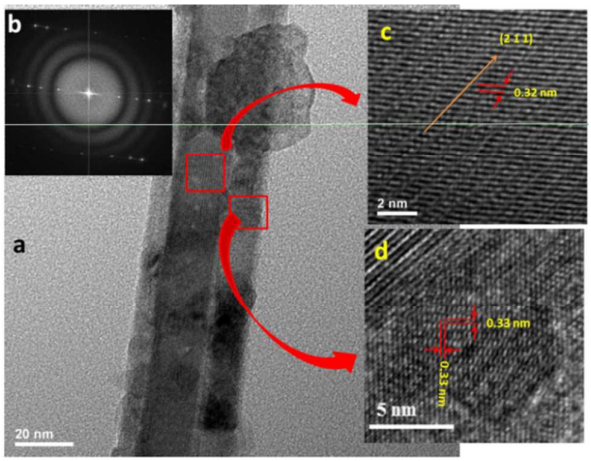

Figure 3:HRTEM image of Bi_2S_3 NW decorated with CdS using 0.01 mole of $Cd(NO_3)_2 \cdot 4H_2O$ (a), Magnified HRTEM image of Bi_2S_3 NW (c), HRTEM image of CdS nanoparticle (d) and SAED pattern of heterostructure (b).

To realize the band structure and the charge carrier transition inside the as-prepared Bi_2S_3 NWs decorated with CdS, the diffuse reflectance (UV-DRS) and Photoluminance spectra of the Bi_2S_3 NWs and Bi_2S_3 NWs decorated with CdS were recorded and analysed.

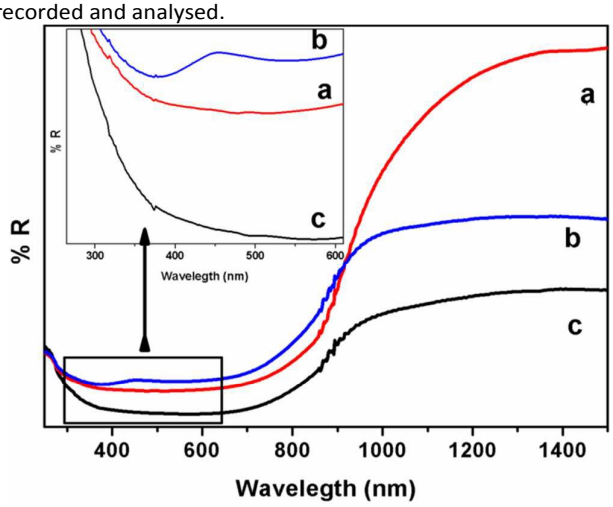

Figure 4 Diffused reflectance spectra of Bi_2S_3 NW decorated with CdS using 0.01 mole of $Cd(NO_3)_2{\cdot}4H_2O$ (a), Bi2S3 NW decorated with CdS using 0.02 mole of $Cd(NO_3)_2 \cdot 4H_2O$ (b)and Bi_2S_3 NW (c)

Figure 4 shows diffuse reflection spectra of Bi_2S_3 NWs and Bi_2S_3 NWs decorated with CdS. Figure 4 shows that the Bi_2S_3 decorated with CdS strong absorption invisible as well as near infarade region. It suggests that these samples have good visible light activity. The band gap values were determined from these spectra by converting the absolute reflection values to the Kubelka–Munk function (F(R)) (see equation 1).[29, 30]

$$F(R) = \frac{(1-R)^2}{2R} \qquad \text{----------} \quad (1)$$

where F(R) is equivalent to the absorption coefficient. figure SII shows plot of F(R) Vs photon energy (hv). As per Kubelka Munk function, band gap energies of Bi_2S_3 NWs (figure 4c) is estimated to be ~ 1.29 eV. The Eg of the and Bi_2S_3 NWs decorated with CdS using 0.01 (figure 4a) and 0.02 mole (figure 4b) of $Cd(NO_3)_2$ is estimated to be 1.31 and 1.37 eV, respectively, which can be attributed to the loading of CdS nanoparticles. It is quite obvious that at higher concentration, the loading of CdS is more with secondary growth. Magnified spectra (inset of Figure 4) clearly shows the broad peak from 450-490nm (2.5eV) which is due to the presence of CdS nanoparticles on Bi_2S_3 NWs.

The charge carrier transition can be also demonstrated by comparing the PL spectra of commercial CdS nanoparticle, Bi_2S_3 NWs and Bi_2S_3 NWs decorated with CdS. As shown in Figure 5, prominent peak in PL spectrum of CdS nanoparticle at~522 nm is becoming weaker for Bi_2S_3 NWs decorated with CdS, suggesting the improved charge carrier separation in the heterostructure.[31, 32]

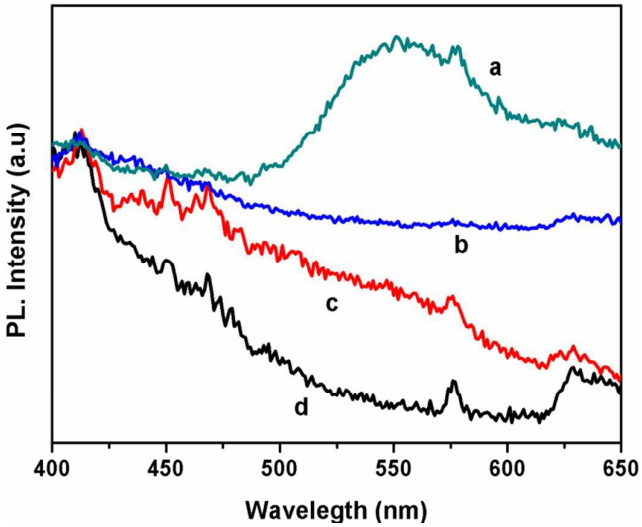

Figure 5 Photoluminescence spectra of commercial CdS (a), Bi_2S_3 NW decorated with CdS using 0.02 mole of $Cd(NO_3)_2 \cdot 4H_2O$ (b), Bi_2S_3 NW decorated with CdS using 0.01 mole of $Cd(NO_3)_2 \cdot 4H_2O$ (c)and Bi_2S_3 NW (d).

Growth Mechanism

As discussed in our previous work,[33] the solvothermal method provides a uniform heating environment under pressure, which results in more simultaneous nucleation than

conventional methods. The solvents and precursors have an influence on the morphologies of the products and favor the synthesis of Bi_2S_3 with different pathways. The formation reaction may be described as follows.

In solvothermal process, the reaction has been occurred in two steps. Bismuth (III) from $BiCl_3$ solution coordinated with the TAA and a dimmer of bismuth (III) sulphide complex has been formed.[34] The probable structure of the complex for bismuth (III) sulphide is presented in Scheme 1.

During the reaction, at the initial stage, the decomposition occurs through the cleavage of the carbon–sulfur bond in Bi-TAA complex clusters and later on the formed Bi_2S_3 nuclei exhibits one dimensional growth and continue to grow along rod-shaped micelles via Ostwald ripening to form one-dimensional Bi_2S_3nanorods or nanowire.

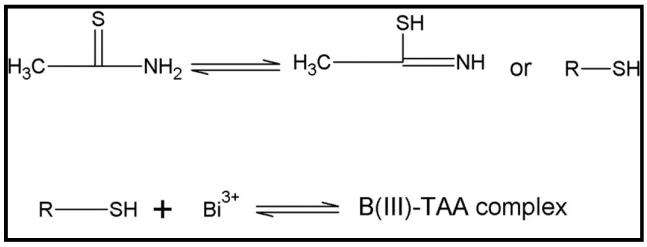

Scheme 1.The formation of dimmer of bismuth (III) sulfide complexes.

The possible reaction mechanism can be proposed as the following.

i) The formation of dimmer of bismuth (III) sulphide complex or B(III)-TAA complexes via coordination reaction between the sulphur and the Bi (III) source at the initial stage of the solvothermal process.

ii) Decomposition of bismuth (III) sulfide complex dimmer and the successive nucleation of Bi_2S_3nanocrystals to form nuclei of Bi_2S_3 nanowires.

iii) Formation of one-dimensional Bi_2S_3 nanowires originated from continuous growth of nucleialong rod-shaped micelles by Ostwald ripening.

Because of the sulfur-alkane structure, TAA is easily transformed into the resonance structure of allylmercaptan with relatively strong nucleophilicity through the resonance. The TAA coordinates to Bi^{3+}ions to form bismuth(III) sulfide complex dimmer with relative stability in the form of allylmercaptan structure (Scheme 1), resulting in low generation rate of S^{2-}. On the other hand, the bismuth (III) sulfide complexes dimmer also has a certain spatial orientation. These two factors are beneficial for the formation of uniform long Bi_2S_3 nanowires (Scheme 2). The CdS is also formed in the same fashion as discussed for Bi_2S_3. According to the K_{sp} of Bi_2S_3 ($1.0X10^{-97}$) and CdS ($8.0X10^{-27}$), Bi_2S_3 will preferentially deposit and form crystal seeds before the formation of CdS. The PVP molecules could attach to some specific crystal facets of the seeds, which limits its growth along [211] direction, and finally confer Bi_2S_3 NWs. However, in the reaction system, the positively charged ions, such as Cd^{2+} and so forth, could weaken the affinity between PVP molecules and nanowires, promote their desorption from the surface of nanowire,[35] and make the following epitaxial growth of CdS nanoparticles possible. Along with the prolonged reaction time, when Bi^{3+} was depleted after that there is an initiation of nucleation process of CdS. The as-produced CdS nanoparticles preferentially deposited at the surfaces of preformed Bi_2S_3 nanowires via epitaxial growth process to reduce their surface energy. Instead of a complete and uniform coating, isolated spherical CdS nanoparticles are formed at the surface of the Bi_2S_3 NWs. As the concentration of the $Cd(NO_3)_2$ increases, the size of decorated CdS nanoparticles also increased. The mobility of ions is quite hastier at higher concentration which leads into fast growth of nanoparticles. Hence, there is a secondary growth of the CdS on surface of Bi_2S_3 NWs as per standard crystal growth mechanism. The scheme 3 represents the growth mechanism of Bi_2S_3 NWs and Bi_2S_3 NW decorated with CdS.

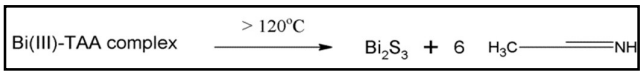

Scheme 2 Pyrolysis of bismuth (III) sulfide complexes dimmer.

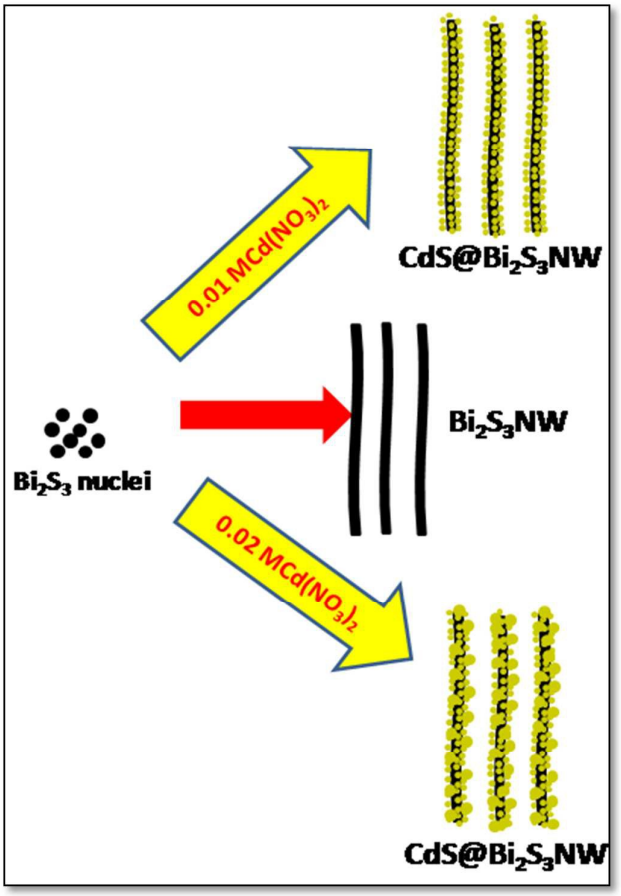

Scheme 3 schematic representation of growth mechanism of Bi_2S_3 NWs and Bi_2S_3 NW decorated with CdS.

Photoresponce study

Figure 6A shows the current–voltage (I-V) plot of prepared Bi_2S_3 NWs and Bi_2S_3 NW decorated with CdS in the dark and under irradiation with white light. Both of these nanostructures showed enhancement of the current flow under white light illumination, Bi_2S_3 NW decorated with CdS showed higher photoconductance. Upon irradiation at 300 W/cm^2, the photocurrent increased approximately from 6.3 X 10^{-6} A/cm^2 to 6.5 X 10^{-5} A/cm^2 (10 times) for Bi_2S_3 NW decorated with CdS, whereas for Bi_2S_3, it increases from 1.10 X 10^{-4} to 1.45 X 10^{-4} A/cm^2 (1.33 times) under similar conditions (at 1 V). This dramatic enhancement was further confirmed by the time dependent photoresponse measurements on both materials at 500 mV (bias voltage) by periodically turning the light on and off (Figure 6B). We obtained considerably high photosensitivity. The current increased by 1 X 10^{-6}A and 15 X 10^{-6}A for Bi_2S_3 NW and Bi_2S_3 W decorated with CdS, respectively in response to the on-and-off operation for duration of 15 s. Even after a number of cycles, the photocurrent could still be changed by illumination switching; thus, the constructed device was fairly stable and reversible.

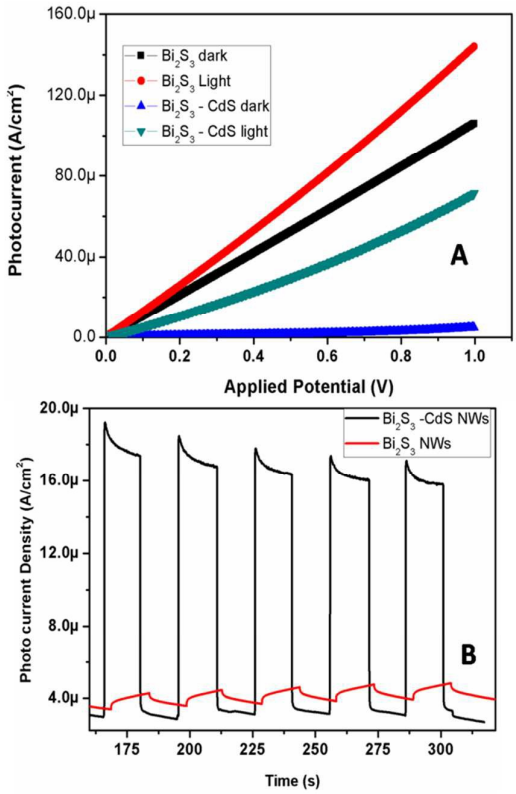

Figure 6 Comparative I–V curves of the Bi_2S_3 NWa and Bi_2S_3 NW decorated with CdS (A) under dark and under light conditions. Time-dependent response of the devices measured in air at a bias of 100 mV.

Bi_2S_3 NWs decorated with CdS prepared by the hydrothermal method creates more structural defects and surface states in materials than bare Bi_2S_3 NWs. Once a material with such defect energy levels is illuminated by light, the photo-generated carriers in it can efficiently be separated. Such spatial separation of the photo-generated carriers reduces the recombination rate of the electron–hole pairs, which in turn causes a significant increase of the carrier density, and thus produces a higher photocurrent.[36, 37]

Photocatalytic hydrogen evolution via H_2S splitting

Considering the good spectral response to solar light, the photocatalytic activities of Bi_2S_3NWs and Bi_2S_3 NWs decorated with CdS nanoparticles for hydrogen evolution from H_2S under solar light have been investigated. Different series of experiments were performed to compare the rate of hydrogen evolution by prepared samples and these results are summarized in Table 1 and Fig. 7. The maximum hydrogen evolution (4560µmol/hr/0.5g) has been obtained using Bi_2S_3 NWs decorated with CdS nanoparticles using 0.01 mole of $Cd(NO_3)_2$ which is higher than that of the Bi_2S_3NWs (3000µmol/hr/0.5g) and Bi_2S_3 NWs decorated with CdS nanoparticles using 0.02 mole of $Cd(NO_3)_2$ (4140 µmol/hr/0.5g), respectively. However, Bi_2S_3 NWs decorated with CdS nanoparticles using 0.01 mole of $Cd(NO_3)_2$ resulted in slightly higher (10%) hydrogen evolution compared with sample Bi_2S_3 NWs decorated with CdS nanoparticles using 0.02 mole of $Cd(NO_3)_2$. Both samples contain CdS nanoparticles interfaced with Bi_2S_3 NWs structures and have good hydrogen evolution. However, slightly lower activity in case of Heterostructure prepared using 0.02 mole of $Cd(NO_3)_2$ is due to the larger CdS particles. The reusability of the Bi_2S_3 NWs decorated with CdS nanoparticles using 0.01 mole of $Cd(NO_3)_2$ as a catalyst for hydrogen generation via H_2S splitting has been tested at same reaction conditions (See Supporting information ESI III). From reusability study, we conclude that our material is more stable after photocatalytic reaction. Surprisingly, it is observed the that the rate of hydrogen generation is higher than the pure CdS nanoparticles and commercial P25. [38-40]

The mechanism of evaluation of hydrogen gas via H_2S splitting is discussed in our previous article in detail.[33] In 0.5 M KOH solution, the weak diprotic acid, H_2S dissociates and maintains equilibrium with the hydrogen disulfide (HS^-) ions. The sulphide semiconductors absorb light and generate electron–hole (e^--h^+) pairs. The valence band hole (h_{VB}^+) photogenerated after the band gap excitation of the Bi_2S_3 powder oxidizes the HS^- ion to the disulfide ion (S_2^{-2}), liberating a proton from the HS^- ion. The conduction band electron (e_{CB}^-) from the Bi_2S_3 photocatalyst reduces the protons to produce molecular hydrogen.[41]

$$H_2S + OH^- \longleftrightarrow 4HS^- + H_2O$$

$$\text{Semiconductor in visible light : } Bi_2S_3 \text{ or } Bi_2S_3/CdS \longleftrightarrow h_{VB}^+ + e_{CB}^-$$

$$\text{Oxidation reaction: } 2HS^- + 2h_{VB}^+ \longrightarrow S_2^{2-} + 2H^+$$

$$\text{Reduction reaction: } 2H^+ + 2e_{CB}^- \longrightarrow H_2$$

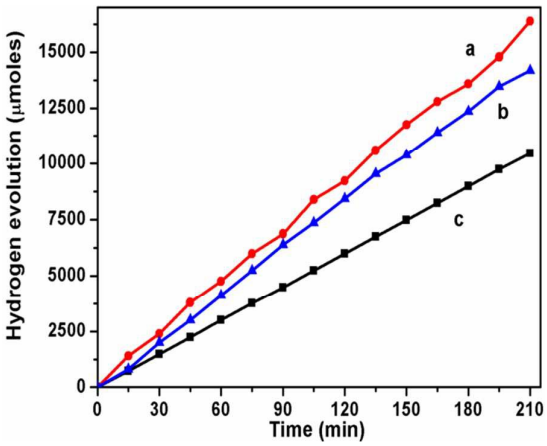

Figure 7 Time dependentHydrogen evolution using Bi_2S_3 NW decorated with CdS using 0.01 mole of $Cd(NO_3)_2$(a), Bi_2S_3 NW decorated with CdS using 0.02 mole of $Cd(NO_3)_2$ (b)and Bi_2S_3 NW (c).

Table 1 Summary of Hydrogen evolution data

Catalyst	Hydrogen Evolution rate (μmole/hr/0.5g)
Bi_2S_3 NW	3000
Bi_2S_3 NWs decorated with CdS nanoparticles using 0.01 mole of $Cd(NO_3)_2$ $4H_2O$.	4560
Bi_2S_3 NWs decorated with CdS nanoparticles using 0.02 mole of $Cd(NO_3)_2$ $4H_2O$.	4140

Hydrogen generation via Glycerol degradation

Photocatalytic hydrogen evolution study was performed using Bi_2S_3 NWs and Bi_2S_3 NWs decorated with CdS catalysts from aqueous glycerol (50% solution) under visible light irradiation. Figure 8 shows the effect of morphology on photocatalytic hydrogen evolution from glycerol. Utmost hydrogen generation i.e. 4.38 mmole $hr^{-1}gm^{-1}$ was observed to be for the Bi_2S_3 NWs decorated with CdS nanoparticles using 0.01 mole of $Cd(NO_3)_2$ $4H_2O$ and 2.34 mmole hr^{-1} gm^{-1} for Bi_2S_3 NWs. The Bi_2S_3 NWs decorated with CdS showed high hydrogen evaluation rate than Bi_2S_3 NWs which may be due to the high surface area and improved charge carrier separation inside the composite i.e. Bi_2S_3 NWs decorated with CdS which ultimately support the enhanced photocatalytic activity. The reason for enhanced photocatalytic activity is already described in above section.

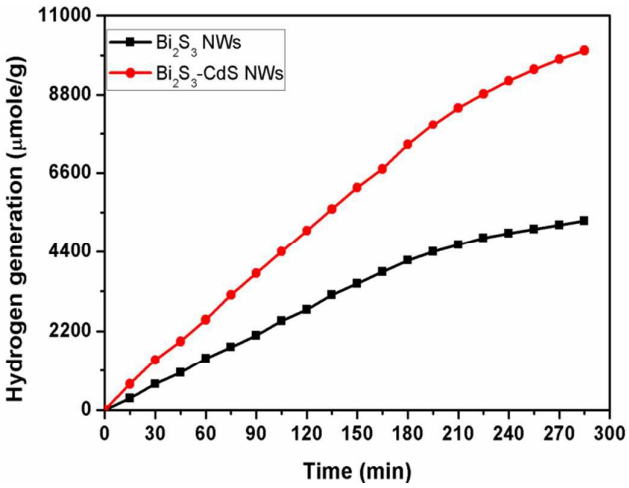

Figure 8 Hydrogen production as a function of irradiation time using Bi_2S_3 NWs and Bi_2S_3 NWs decorated with CdS

Photocatalytic production of hydrogen from glycerol–water mixture consists of two distinct mechanisms, that is, photo-splitting of water and photo-reforming of glycerol.[42] First, glycerol is oxidized, and then, it produces several intermediate compounds followed by hydrogen as product. Second, glycerol acts as sacrificial agent in photocatalytic water splitting [43] Glycerol, which acts as a sacrificial electron donor, is to rapidly remove the photo-generated holes (hydroxyl radicals) and/or photo-generated oxygen in an irreversible fashion, thereby suppressing electron-hole recombination and/or H_2–O_2 back reaction. By doing so, glycerol is progressively oxidized toward CO_2, with intermediate formation of partially oxidized products. When complete oxidation of glycerol (and reaction intermediates) is achieved, oxygen can no longer be removed from the photocatalyst surface and the rate of hydrogen production drops to steady-state values comparable to those obtained in the absence of glycerol in solution.

The overall process, which may be described as photo-induced reforming of glycerol at room temperature, can be expressed by the following equation, which predicts the observed H_2: CO_2 = 7:3 molar ratio of products formed:

$$C_3H_8O_3 + 3H_2O \longrightarrow 3CO_2 + 7H_2 \qquad (2)$$

Photocatalytic Methylene Blue degradation

Methylene blue (MB) dye is used in textile industries massively and hence is of the major source of water pollution. Characteristic absorption peak of methylene blue appears at around 663. This absorption peak have been used to monitor the photocatalytic degradation process.[44,45] The photodegradation efficiencies of MB mediated by the Bi_2S_3 NWs and Bi_2S_3 NWs decorated with CdS nanoparticls as photocatalyst as well as without photocatalyst under visible-light illumination (λ> 400 nm) are displayed in Figure 9. Figure 8 alsoshows the $\ln(C/C_0)$ as a function of time under visible light (λ>400 nm) irradiation, where C is the concentration of MB at the irradiation time t and C_0 is the concentration in the adsorption equilibrium of the photocatalysts before irradiation.

The degradation rate of dyes is expressed as degradation-rate constant *k* which is summarized in Table 2.

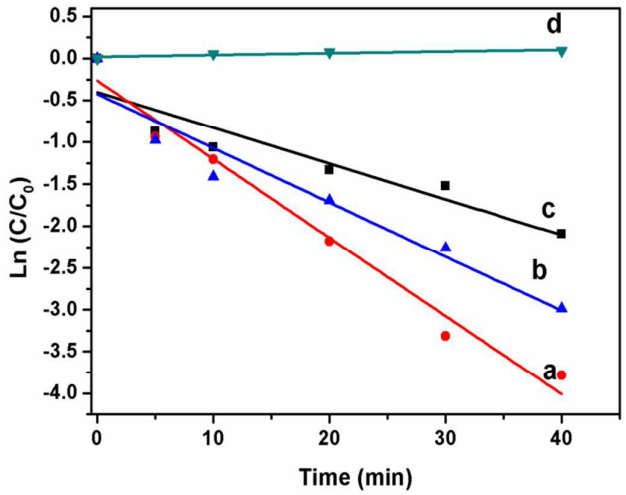

Figure 9 Photocatalytic degradation of MB (initial concentration 1.0 X10^{-5} M) using Bi_2S_3 NW decorated with CdS using 0.01 mole of $Cd(NO_3)_2$(a), Bi_2S_3 NW decorated with CdS using 0.02 mole of $Cd(NO_3)_2$ (b), Bi_2S_3 NW (c) and without catalyst .

Table 2 Reaction rate constant *k* for dye degradation

Catalyst	Rate constant (*k*)
Bi_2S_3 NWs	-0.042
Bi_2S_3 NW decorated with CdS using 0.01 mole of $Cd(NO_3)_2$	-0.094
Bi_2S_3 NW decorated with CdS using 0.02 mole of $Cd(NO_3)_2$	-0.065
Without catalyst	0.002

Rate constant obtained for different nanostructures indicates that the photocatalytic performances are strongly dependent on shape, size, and structure. The Bi_2S_3 NW decorated with CdS using 0.01 mole of $Cd(NO_3)_2$ showed higher photocatalytic activity for the degradation of MB Bi_2S_3 NWs as well as Bi_2S_3 NW decorated with CdS using 0.02 mole of $Cd(NO_3)_2$ as shown in Figure 9 and Table 2. The enhanced photocatalytic activity Bi_2S_3 NWs decorated with CdS nanoparticles can be attributed due to creation of more the structural defects and surface states in materials than bare Bi_2S_3 NWs

Figure SI-IV (See supporting information EIS IV) reveals the temporal evolution of the absorption spectra of an MB aqueous solution catalysed by the Bi_2S_3 NWs and Bi_2S_3 NWs decorated with CdS under visible light irradiation (λ>400 nm)

Possible mechanism of the enhancement of photocatalytic activity of Bi_2S_3 NWs Decorated with CdS photocatalyst

It is well reported that the photocatalytic activity is depend of some vital factors such as optical absorption, adsorption ability, phase structure and separation efficiency of photo-generated charge carriers.[46, 47] However, it is necessary to find out the band edge positions of the valence band (VB) and conduction band (CB) of both Bi_2S_3 and CdS to understand the photocatalytic reaction mechanism because they have strong relation with the photocatalytic Redox process. The valence band potentials and conduction band potential of Bi_2S_3 and CdS were calculated according to the following empirical equations:[48]

$$E_{VB} = \chi - E_{fe} + \frac{1}{2}E_g \quad \text{---------- (3)}$$

$$E_{cB} = \chi - E_{fe} - \frac{1}{2}E_g \quad \text{---------- (4)}$$

where E_{VB} and E_{CB} are the valence band and conduction band edge potentials respectively, χ is the electronegativity of the semiconductor, which is the geometric mean of the electronegativity of the constituent atoms. As per literature, the values of χ for Bi_2S_3 and CdS have been calculated as 5.27 eV and 5.04 eV, respectively.[49-51] E_{fe} is the energy of free electrons on the hydrogen scale (about 4.5 eV) and E_g is the band gap energy of the semiconductor. The band gap of Bi_2S_3 and CdS is about 1.32 and 2.40 eV, respectively. On the basis of band gap positions, the band edge potentials of VB and CB for Bi_2S_3 are 1.43 eV and 0.11 eV while for CdS are 1.72 eV and -0.66 eV, respectively.

Based on above valus and our phtocatalysis results, a possible mechanism for enhanced photocatalytic activity based on photo-carrier transfer is shown in Scheme 4.

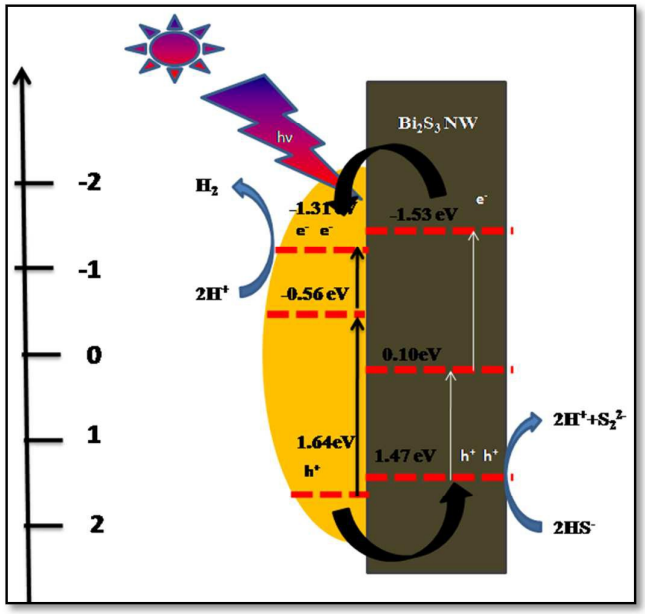

Scheme 4 Schematic representation of photocatalytic hydrogen generation using Bi_2S_3 NWs decorated with CdS nanoparticles.

In the presence of solar light irradiation, both Bi_2S_3 and CdS with band gap 1.37 and 2.40 eV can be photo-excited up to higher potential edge i.e. -1.53 and -1.31 eV for Bi_2S_3 and CdS due to the higher photon energy.[52, 53] However, bare Bi_2S_3 NWs nanorods show poor photocatalytic activity on expenses of the high recombination of the photoinduced carriers. In the case of Bi_2S_3 NWs decorated with CdS, due to higher conduction band

potential (E_{CB}) of Bi_2S_3 NWs compared to that of CdS, the transfer of the photo-excited electrons from the surface of Bi_2S_3 NWs to CdS nanoparticles take place. Simultaneously, the photo-excited holes created by the visible light irradiation on CdS can also migrate to the Bi_2S_3 NWs surface and react with the HS- ions. This transfer of electron–hole subsequently reduces the recombination of electrons and holes. The reduction of recombination admits more chances for electrons to participate in the reduction reaction to form H_2 molecules which leads to a higher photocatalytic activity and excellent stability. Yet, with an increase in the amount of CdS, the excessive photoinduced electrons and holes can unavoidable recombine thus, decrease the photoactivity. The recombination of electron hole pair is also discussed in photoluminescence study. The optimized Bi_2S_3 NWs decorated with CdS prepared using 0.1 M $Cd(NO_3)_2$ which showed the best photocatalytic activity.

Conclusions

In nutshell, Bi_2S_3 NWs decorated with CdS nanoparticles have been successfully synthesized in solution phase at mild temperature. The growth mechanism of the formation of the nanoscale heterostructure has also been discussed. The prepared nanoscale heterostructure exhibits superior photocatalytic hydrogen generation activity and is strongly dependent on its composition and microstructure. Experimental studies reveal that the size of the CdS nanoparticle determines the band gap energy of the nanoscale heterostructure, controlling the charge carrier transition, recombination and separation in heterostructure. Hence the Bi_2S_3 NWs decorated with CdS showed an efficient hydrogen generation rate than bare Bi_2S_3 NWs. The enhanced photocatalytic results indicate potential application of nanoscale chalcogenide heterostructures in organic waste degradation**.** The methodology can also be extended to the preparation of other nanoscale heterostructures.

Acknowledgements

The authors would like to thank, Executive Director, C-MET, Pune for technical support and DeitY, New Delhi financial support.

Notes and references

‡Footnotes relating to the main text should appear here. These might include comments relevant to but not central to the matter under discussion, limited experimental and spectral data, and crystallographic data.

.

1 H. Li, J. Yang, J. Zhang and M. Zhou, *RSC Advances*, 2012, **2,** 6258.
2 X. H. Lu, G. M. Wang, T. Zhai, M. H. Yu, J. Y. Gan, Y. X. Tong and Y. Li, *Nano Lett.*2012, **12**, 1690.
3 B. Cheng, G. Wu, Z.Ouyang, X. Su, Y. Xiao and S. Lei, ACS *Appl. Mater. Interfaces*, 2014, **6**, 4057.
4 L. Li, Y. W. Yang, G. H. Liand L. D. Zhang, *Small* 2006, **2**, 548.
5 L. Hu,J.Yan , M. Liao , H. Xiang, X.Gong, L.Zhang and X. Fang,*Adv. Mater*. 2012, **24,** 2305.
6 S. Liu, J. F. Ye, Y. Cao, Q. Shen, Z. F. Liu, L. M. Qi, X. F. Guo*, Small* 2009, **5**, 2371.
7 X. Zhang, Y. Liu and Z. Kang, *ACS Appl. Mater. Interfaces*, 2014, **6**, 4480.
8 Y-C. Pu, G. Wang, K-D. Chang, Y. Ling, Y-K. Lin, B. C. Fitzmorris, C-M. Liu, X.Lu, Y.Tong, J. Z. Zhang, Y-J. Hsu, Y. Li, *Nano Lett*. 2013, **13**, 3817.
9 X.Zhang, Y. Liu and Z. Kang, *ACS Appl. Mater. Interfaces,*2014, 6, 4480.
10 Z.-Q. Liu, W.-Y. Huang, Y.-M. Zhang and Y.-X. Tong, *CrystEngComm*, 2012, **14**, 8261.
11 H.-P. Jiao, X. Yu, Z.-Q. Liu, P.-Y. Kuang, and Y.-M. Zhang, *RSC Adv.*, 2015, **5**, 16239.
12 M. Hara.G. Hitoki, T. Takata, J. N. Kondo, H. Kobayashi andK. Domen,*Catal Today,*2003, **78**, 555.
13 X. Zong, H. J. Yan, G. P. Wu, G. J. Ma, F. Y. Wen, L. Wang and C. Li,*J Am Chem. Soc.*2008, **130**, 7176.
14 W. Li, S. Xie, M. Li, X.Ouyang, G.Cui, X. Lu and Y.Tong, *J. Mater. Chem. A,* 2013, **1**, 4190.
15 P. Tongying, F. Vietmeyer, D. Aleksiuk, G. J. Ferraudi, G. Krylova and M. Kuno, *Nanoscale*, 2014,**6**, 4117.
16 P.Tongying, V.V. Plashnitsa, N.Petchsang, F.Vietmeyer, G. J. Ferraudi, G.Krylova and M. Kuno, *J. Phys. Chem. Lett*.2012, **3,** 3234.
17 H. Kim, M. Seol, J. Lee and K.Yong, *J. Phys. Chem. C*, 2011, **115**,25429.
18 Z.Fang, Y.Liu, Y.Fan, Y.Ni, X.Wei, K.Tang, J.Shen and Y.Chen, *J. Phys. Chem. C,* 2011, **115**, 13968.
19 J. S. Jang, H. G. Kim, U. A. Joshi, J. W. Jang and J. S. Lee, *Inter. J. Hyd. Energy*, 2008,**33,** 5975.
20 J. Hou, C.Yang, Z.Wang, S. Jiao and H.Zhu, *RSC Adv.* 2012, **2**, 10330.
21 X. Wang, G. Liu, Z-G. Chen, F. Li, L.Wang, G. Q. Lu and H-M. Cheng, *Chem. Commun*. 2009, 3452.
22 Z. Fang, Y. Liu, Y. Fan, Y.Ni, X. Wei, K.Tang, J. Shen and Y.Chen, *J. Phys. Chem. C*, 2011, **115**, 13968.
23 A. Jana, C. Bhattacharya and J. Datta, *Electrochim. Acta*, 2010, **55**, 6553.
24 X. He, L.Gao, S. Yang and J.Sun, *CrystEngComm*, 2010, **12,** 3413.
25 K. M. Gadave, C. D. Lokhande andP. P. Hankare, *Mater. Chem. Phys.*1994, **38,** 393-397.
26 N. Soltania, E. Saiona, W. M. M. Yunusa, M. Navaserya, G. Bahmanrokha, M. Erfania, M.R. Zareb, E. Gharibshahia, *Solar Energy,* 2013, **97**, 147.
27 F. Zhang, S. S. Wong, *Chem. Mater*. 2009, **21**, 4541.
28 T. Wu, X. G. Zhou, H. Zhang, X. H. Zhong, *Nano Res.*2010,**3,** 379.
29 Y. I Kim, S. J. Atherton, E. S. Brigham and T. E. Mallouk, *J. Phys. Chem. B,* 1993, **97**, 11802.
30 A B Murphy, *J. Phys. D: Appl. Phys*. 2006, **39**, 3571.
31 R. P. Panmand, Y. A. Sethi,S. R. Kadam,M. S. Tamboli, L. K. Nikam,J. D. Ambekar,C.-J. Park andB. B. Kale, *CrystEngComm,* 2015,**17,** 107.
32 N.S. Chaudhari,S. S. Warule,S.A. Dhanmane, M. V. Kulkarni, M. Valant andB. B. Kale, *Nanoscale,* 2013,**5,** 9383.
33 U. V. Kawade, R. P. Panmand, Y. A. Sethi,M. V. Kulkarni, S. K. Apte,S. D. Naik andB. B. Kale, *RSC Adv,* 2014,**4**, 49295.
34 W. Xiang, Y. Yang, J. Yang, H. Yuan, J. An, J. Wei and X. Liu, *J. Mater. Res,* 2014, **29**, 2272.
35 A. Z. Zelikin, G. K. Such, A. Postma and F. Caruso, *Biomacromolecules,*2007, **8,** 2950
36 W. Tian, C. Zhang, T. Zhai, S.-L. Li, X. Wang, J. Liu, X. Jie, D. Liu, M. Liao, Y. Koide, D. Golberg, and Y. Bando, *Adv. Mater.* 2014, **26,** 3088.
37 C. Zhang, W. Tian, Z. Xu, X. Wang, J. Liu, S.-L. Li, D.-M. Tang, D. Liu, M. Liao, Y. Bando and D. Golberg, Nanoscale, 2014, 6, 8084–8090

38 B. B. Kale, J.-O. Baeg, S. K. Apte, R. S. Sonawane, S. D. Naik and K. R. Patil, *J. Mater. Chem.*, 2007, **17**, 4297-4303.
39 S. N Garaje, S. K Apte, S.i D Naik, J. D Ambekar, R. S Sonawane, M. V Kulkarni, A. Vinu, B. B Kale, *Environ. Sci. Technol.*, 2013, **47,** 6664–6672.
40 N. S Chaudhari, S. S Warule, S. A Dhanmane, M. V Kulkarni, M. Valant, B. B Kale, *Nanoscale*, 2013,**5**, 9383-9390.
41 B. B. Kale, J. O. Baeg, K. Kong, S. Moon, L. K. Nikam and K. R. Patil, *J. Mater. Chem.* 2011, **21,** 2624.
42 J. Jitputti, Y. Suzuki, S. Yoshikawa, *CatalCommun*. 2008, **9**, 1265.
43 V. Gombac, L. Sordelli,T. Montini, J. J. Delgado, A. Adamski, G. Adami, M. Cargnello, S. Bernal, P. Fornasiero; *J. Phys. Chem. A,* 2010, **114**, 3916.
44 Z. Liu, F. Chen, Y. Gao, Y. Liu, P. Fang, S. Wang, *J. Mater. Chem. A*, 2013, **1**, 7027.
45 G. Zhao, S. Liu, Q. Lu, and L. Song, *Ind. Eng. Chem. Res.* 2012, **51,** 10307.
46 I. Aslam, C. Cao, M. Tanveer, M. H. Farooq, W. S. Khan, M. Tahir, F. Idrees and S. Khalid, *RSC Adv*., 2015, **5**, 60190,
47 J. Xu, M. Chen and Z. Wang, *Dalton Trans*., 2014, **43**, 3537.
48 Y. Xu and M. A. Schoonen, *Am. Mineral*., 2000, **85**, 543.
49 Y. Yan, Z. Zhou, W. Li, Y. Zhu, Y. Cheng, F. Zhao and J. Zhou, *RSC Adv*., 2014, **4,** 38558.
50 L. Wang, W. Wang, *CrystEngComm*, 2012, **14**, 3315.
51 R. G. Pearson, Inorg. Chem., 1988, 27, 734.
52 J. Chen, S. Qin, G. Song, T. Xiang, F. Xin and X. Yin, *Dalton Trans.*, 2013, **42**, 15133.
53 M. R. Gholipour, C.-T. Dinh, F. Bélandb and T.-O Do, *Nanoscale*, 2015, **7,** 8187.

In-situ fabrication of highly crystalline CdS decorated Bi2S3 nanowires (Nano-Heterostructure) for visible light photocatalyst application

Rajendra P. Panmanda, Yogesh A. Sethia, Rajashree S. Deokarb, Datta J. Latec, Haribhau M. Gholapb, Jin Ook Baegd and Bharat B. Kalea***

Herein, we have demonstrated the In-situ synthesis of the orthorhombic Bi_2S_3nanowiresdecorated with hexagonal CdS nanoparticles (nano-heterostructure) by facile solvothermal method. The heterostructures have been used as photocatalyst for hydrogen production under solar light.